PHYSICAL REVIEW B VOLUME 25, NUMBER 12 15 JUNE 1982

Anomalous paramagnetic neutron spectra of some intermediate-valence compounds

E. Holland-Moritz and D. Wohlleben
II. Physikalisches Institut der Universität Köln, West Germany

M. Loewenhaupt
Institut für Festkörperphysik, Kernforschungsanlage Jülich, West Germany

(Received 6 August 1981)

Magnetic neutron spectra as a function of temperature are presented for the intermediate-valence compounds $CePd_3$, $CeSn_3$, $CeBe_{13}$, $YbCu_2Si_2$, and TmSe. All compounds show the normal local $4f$ form factor but a broadened magnetic energy spectrum with an overall width of about 7 to 30 meV and with very little temperature dependence (except TmSe). Closer analysis reveals a residual crystal-field spectrum in $YbCu_2Si_2$ which may also underlie the spectra of the other compounds. A detailed description of the data analysis is given.

I. INTRODUCTION

The present paper describes an extended investigation of the energy dependence of the paramagnetic neutron cross section of several intermediate-valence compounds. Some results of this investigation have appeared in preliminary form elsewhere.[1–5]

Certain intermetallic rare-earth (RE) compounds exhibit the so-called intermediate-valence (IV) or valence fluctuation phenomenon. A large body of data suggests that in such compounds two neighboring ionic configurations of the $4f$ shell are involved in an essential way. For instance, L_{III} x-ray absorption spectra[6] and x-ray photoemission spectra[7] clearly demonstrate the coexistence of two ionic configurations in two resolved, corresponding spectra. On the other hand, the Mössbauer spectrum shows a single peak at an intermediate position rather than two peaks corresponding to the respective normal configurational isomer shifts.[8] The Mössbauer result excludes static coexistence of the two configurations. It follows that the mixture must be dynamic with a mixing energy intermediate between the configurational energy differences observed in the x-ray (1 eV) and the Mössbauer (10^{-6} eV) measurements.[9] With the exception of TmSe, all known intermediate-valence compounds are paramagnetic at $T\rightarrow 0$ K. This conclusion follows from the behavior of the static susceptibility, from the absence of hyperfine splitting in the Mössbauer spectra, and from the absence of magnetic Bragg peaks in the neutron data.

On the other hand, the static susceptibility often shows a large negative paramagnetic Curie-Weiss temperature and a broad maximum near a temperature whose value far exceeds the possible magnetic ordering temperature. This effective temperature is therefore interpreted as a measure of the effective mixing energy.

The configurational mixing process via emission and absorption of a conduction electron leads to local magnetic and charge fluctuations with in general different time scales.[10,11] Such fluctuations can be observed experimentally by inelastic scattering of appropriate probes (neutrons, electrons, or photons) in the energy range of the fluctuations. Judging from the static susceptibility the magnetic fluctuation energy is a few hundred Kelvin or less. This makes inelastic magnetic neutron scattering of thermal neutrons an ideal tool to measure the magnetic fluctuation spectra of IV compounds. Thermal neutrons do not only have the right energy range, but also a nearly ideal wavelength (2 Å) at that energy for optimal spatial coupling to the local $4f$ magnetization which varies in space over distances of order 0.5 Å.

Since IV compounds are usually paramagnetic at $T\rightarrow 0$ K, one may take the magnetic spectrum of stable $4f$ shells in the high-temperature regime as a guide to predict the qualitative behavior of the magnetic IV spectra. In general, the paramagnetic regime is characterized in the neutron cross section by quasielastic Lorentzians centered at $\hbar\omega=0$ and by inelastic crystal-field (CEF) transition lines. The temperature dependence of the quasielastic linewidth of the CEF ground state of a stable $4f$ shell at temperatures small compared to the energy of the first-excited CEF state is given by the Korringa relation[12] $\Gamma/2(T)=\alpha k_B T$ with α of order

$10^{-4}-10^{-2}$, i.e., the linewidth of the low-temperature paramagnetic spectrum is usually very small compared to the thermal energy. At intermediate temperatures the spectrum becomes complicated, but should merge into a broad Lorentzian again at sufficiently high temperatures.[13] The linewidth is due to the interaction with the conduction electrons. In the configurational mixing process this interaction is especially strong and temperature independent at low temperatures. We therefore expect the paramagnetic neutron scattering to look similar to that from the stable $4f$ configuration, but with exceptionally large and essentially temperature-independent linewidth.

The experiments reported here and previously[1-5] were undertaken to detect this large abnormal temperature dependence of the paramagnetic neutron scattering cross section. This paper describes the original data on $CePd_3$ (Ref. 1) in more detail and reports similar measurements on several other systems: $CeSn_3$, $CeBe_{13}$, and $YbCu_2Si_2$. Moreover, the magnetically ordering compound TmSe was studied with respect to its paramagnetic behavior above 4 K.

II. THEORY

The paramagnetic scattering law for unpolarized neutrons is given by[14,15,2]

$$S(\vec{Q},\hbar\omega,T)=\frac{1}{2\pi}\left[\frac{g_N r_e}{\mu_B}\right]^2\chi''(\vec{Q},\hbar\omega,T)\times\frac{1}{1-\exp(-\beta\hbar\omega)}=\frac{k_0}{k_1}\frac{d^2\sigma}{d(\hbar\omega)d\Omega}\ . \tag{1}$$

Here S is the scattering amplitude per magnetic ion, $d^2\sigma/d(\hbar\omega)d\Omega$ the double differential cross section, $g_N=-1.91$, $r_e=2.8\times10^{-13}$ cm is the classical electron radius, $\mu_B=e\hbar/mc$ the Bohr magneton, $\beta=(k_BT)^{-1}$, and $\hbar\omega=E_0-E_1$. E_0 is the energy of the incident and E_1 the energy of the scattered neutrons (for the neutron energy gain $\hbar\omega$ is negative). $\chi''(\vec{Q},\hbar\omega,T)$ is the imaginary part of the dynamic susceptibility (per magnetic ion). For incident energies sufficiently small compared to Hund's rule, spin-orbit coupling the Kramers-Kronig relation gives a relationship which can be written as follows:

$$\chi''(\vec{Q},\hbar\omega,T)=\chi'(\vec{Q},0,T)P(\vec{Q},\hbar\omega,T)\hbar\omega\pi\ . \tag{2}$$

Here $P(\vec{Q},\hbar\omega,T)$ is a spectral function which must fulfill the relation

$$\int_{-\infty}^{\infty}P(\vec{Q},\hbar\omega,T)d(\hbar\omega)=1\ , \tag{3}$$

and $\chi'(\vec{Q},0,T)$ is the static susceptibility which can be factorized as

$$\chi'(\vec{Q},0,T)=F^2(\vec{Q},T)\chi'(0,0,T)\ , \tag{4}$$

where $F(\vec{Q},T)$ is a magnetic form factor and $\chi'(0,0,T)=\chi_{st}(T)$ is the static bulk susceptibility as measured in a Faraday magnetometer. The separation of the dynamic susceptibility into the static susceptibility and the spectral function [Eq. (2)] is more complicated for the crystal-field case (see Sec. II D). One can define a local magnetic moment p_{loc} by writing

$$\chi_{st}(T)=p_{loc}^2(T)\mu_B^2A(T)\ . \tag{5}$$

Finally with (1), (2), and (4) one can write the scattering amplitude as

$$S(\vec{Q},\hbar\omega,T)=\frac{1}{2}\left[\frac{g_N r_e}{\mu_B}\right]^2F^2(\vec{Q},T)\chi_{st}(T)\times P(\vec{Q},\hbar\omega,T)\frac{1}{1-e^{-\beta\hbar\omega}}\hbar\omega\ , \tag{6}$$

or with (5) as

$$S(\vec{Q},\hbar\omega,T)=\tfrac{1}{2}(g_N r_e)^2F^2(\vec{Q},T)p_{loc}^2(T)\times P(\vec{Q},\hbar\omega,T)\frac{A(T)\hbar\omega}{1-e^{-\beta\hbar\omega}}\ . \tag{7}$$

We will define the *total magnetic cross section* (bulk) by

$$\sigma_{mag}=4\pi\int_{-\infty}^{\infty}d(\hbar\omega)S(Q=0,\hbar\omega,T) \tag{8}$$

and the local magnetic cross section Σ_{loc} by replacing the bulk susceptibility by the local part only, i.e., that fraction of σ_{mag} which one obtains by extrapolating the local magnetic form factor to $Q=0$. Let us discuss three special cases of RE ions without crystal-field splitting and finally the crystal-field case.

A. Curie case

The Curie susceptibility of a stable RE ion in a metal is given by

$$\chi_{st}(T)=g_J^2J(J+1)\mu_B^2/3k_BT\ . \tag{9}$$

Here J and g_J are the total angular momentum and

the Landé g factor of the Hund's rule ground state. This formula is valid in the absence of crystal-field splittings when the thermal energy is small compared to the intraconfigurational multiplet splitting, and when ion-ion interactions are negligible. In this case

$$p_{\rm loc}^2 = g_J^2 J(J+1) \tag{10}$$

and the spectrum is a Lorentzian centered at $\hbar\omega = 0$ with a width given by the Korringa relation

$$\Gamma/2(T) = 4\pi[N(E_F)J_{\rm ex}(g_J-1)]^2 k_B T \equiv \alpha k_B T \ . \tag{11}$$

$J_{\rm ex}$ is the exchange integral and $N(E_F)$ is the density of conduction-electron states at the Fermi level. Usually

$$N(E_F)J_{\rm ex}(g_J-1) \simeq 10^{-2} << 1 \ ,$$

so that on an energy scale $k_B T$ the spectral function $P(\vec{Q},\hbar\omega,T)$ behaves nearly like a δ function and the total magnetic cross section becomes, with

$$\hbar\omega/[1-\exp(-\beta\hbar\omega)] \to 1/\beta$$

and Eqs. (6) and (8)–(10),

$$\sigma_{\rm mag} = 4\pi \frac{1}{2}\left[\frac{g_N r_e}{\mu_B}\right]^2 \chi_{\rm st}(T) k_B T$$

$$= 4\pi \tfrac{1}{6}(g_N r_e)^2 p_{\rm loc}^2$$

$$= \Sigma_{\rm loc} \ . \tag{12}$$

Here the local magnetic cross section is independent of temperature as long as $p_{\rm loc}$ does not depend on temperature. Note that in this case the total magnetic cross section is identical to the local magnetic cross section [Eq. (12)] and independent of temperature in accordance with the fact that in the Curie case the bulk susceptibility is equivalent to the local susceptibility.

B. Curie-Weiss case

If magnetic interactions between the ions are present, the susceptibility shows Curie-Weiss behavior in the paramagnetic region, i.e.,

$$\chi_{\rm st}(T) = p_{\rm loc}^2 \mu_B^2 / 3k_B(T-\Theta) \ , \tag{9'}$$

where $p_{\rm loc}$ is given by Eq. (10) and Θ is the Curie-Weiss temperature. For temperatures large compared to the ordering temperature, the linewidths $\Gamma/2$ of the Zeeman levels are still small compared to the thermal energy $k_B T$. The first part of Eq. (12) is still valid, and the total magnetic cross section becomes

$$\sigma_{\rm mag} = 4\pi \tfrac{1}{6}(g_N r_e)^2 p_{\rm loc}^2 T/(T-\Theta)$$

$$= \Sigma_{\rm loc} T/(T-\Theta) \ . \tag{12'}$$

Since the total magnetic cross section $\sigma_{\rm mag}$ as well as the static bulk susceptibility are defined for $Q \to 0$, the relationship between $\sigma_{\rm mag}$ and $\chi_{\rm st}$ will be the same as in the Curie case [Eq. (12)]. However, in the Curie-Weiss case there is now a difference between the total magnetic cross section $\sigma_{\rm mag}$ ($Q \to 0$) and the local magnetic cross section $\Sigma_{\rm loc}$ [Eq. (12')]. In the presence of interactions local correlations exist between neighboring ions even in the paramagnetic region. These correlations between neighbors are temperature dependent and will cause deviations of the measured form factor $F^2(Q)$ from the free-ion form factor (local form factor) in the region $Q < 1/a$ (where a is the nearest-neighbor distance), i.e., near $Q \to 0$, but not for large Q values.

In the case of ferromagnetic (antiferromagnetic) short-range interactions the paramagnetic bulk susceptibility is larger (smaller) than the local susceptibility expected for a free local moment. The difference is given by the factor $T/(T-\Theta)$ with $\Theta > 0$ ($\Theta < 0$). Similarly, the measured form factor will increase (decrease) for $Q \to 0$ in those systems compared to the local form factor. Therefore in the Curie-Weiss case the scattered intensity for local measurements is not given by the static bulk susceptibility as described by Eq. (12), but with Eqs. (9') and (12') by

$$\Sigma_{\rm loc} = 4\pi \frac{1}{2}\left[\frac{g_N r_e}{\mu_B}\right]^2 \chi_{\rm st} k_B (T-\Theta)$$

$$= 4\pi \tfrac{1}{6}(g_N r_e)^2 p_{\rm loc}^2 \ . \tag{13}$$

While the local magnetic cross section is temperature independent (as long as the local magnetic moment is temperature independent), the total magnetic cross section becomes temperature dependent [Eq. (12')], which is due to the temperature dependence of the form factor.

C. IV case

In the IV compounds three questions were open before starting our experiments:

(1) Is the anomalous static bulk susceptibility mainly of local nature?

(2) What is the energy dependence of this local scattering?

(3) Can one obtain some information about the valence of the IV ion by neutron scattering?

In IV compounds the quasielastic linewidth $\Gamma/2$ becomes larger than the thermal energy $k_B T$ for temperatures smaller than the so-called fluctuation temperature T_{SF} (to be seen later). Then the quasielastic line can no longer be approximated by a δ function. Therefore the local cross section must be described by the full expression

$$\Sigma_{loc}=2\pi\left[\frac{g_N r_e}{\mu_B}\right]^2 \chi_{loc}(T) \times \int_{-\infty}^{\infty} \frac{\hbar\omega}{1-e^{-\beta\hbar\omega}} P(\vec{Q},\hbar\omega,T)d(\hbar\omega) . \tag{14}$$

The local susceptibility χ_{loc} can be obtained by fitting the neutron scattering measurements with Eq. (6) using the local magnetic form factor and assuming, for instance, a Lorentzian spectral function. The values obtained in this way can then be compared with the bulk susceptibility measured in a Faraday magnetometer.

To obtain a value for the valence one has to know the local magnetic cross section, i.e., one has to perform a measurement of the cross section at all energies, or, since this is impossible (our measurements do not extend beyond 50 meV of incoming energy or beyond about 30 meV of energy gain for $T=300$ K), one has to calculate the local magnetic cross section by solving the integral in Eq. (14) with a spectral function, which makes certain assumptions about the energy dependence at experimentally inaccessible high-energy regions. For the latter procedure one may assume a Lorentzian, but this spectrum is physically unrealistic at very high energy transfers. Analytically the temporal correlation function $e^{-|t|/\tau}$ underlying the Lorentzian power spectrum has a singular derivative at $t=0$ which causes the integral over the first moment of the power spectrum $\hbar\omega P(\hbar\omega)$ to diverge. Physically this high-energy region is not described properly by the exponential correlation function because it implies that parts of the system can move arbitrarily fast. A natural cutoff for the Lorentzian at high energies would be the bandwidth of the conduction electrons, which unfortnately is unknown. Another procedure to mend the difficulties with the Lorentzian is to use a Gaussian at high energies. We have analyzed the data either with a cutoff or with a combination of a Lorentzian at low energies and a Gaussian at high energies.

D. CEF case

As already mentioned at the beginning of Sec. II [after Eq. (4)] the scattering law [Eq. (6)] must be modified for inelastic transitions, e.g., CEF transitions. This can be done by splitting the static susceptibility into Curie and Van Vleck terms:

$$\frac{\hbar\omega}{1-e^{-\beta\hbar\omega}}\frac{1}{\mu_B^2}\chi_{st}P(Q,\hbar\omega,T) \tag{15a}$$

$$\rightarrow \frac{\hbar\omega}{1-e^{-\beta\hbar\omega}}\frac{1}{\mu_B^2}\left[\sum_m \chi_c^m P_{mm}(Q,\hbar\omega,T)+\tfrac{1}{2}\sum_{m\neq n}\chi_{VV}^{mn}(1-e^{-\beta\Delta_{nm}})P_{nm}(Q,\hbar\omega-\Delta_{nm},T)\right] . \tag{15b}$$

Here

$$\chi_c^m=\frac{\mu_B^2}{k_B T}g_J^2\rho_m |\langle m|J_z|m\rangle|^2 , \tag{16}$$

is the Curie susceptibility of the mth level and

$$\chi_{VV}^{nm}=2\mu_B^2 g_J^2\rho_m\frac{|\langle n|J_z|m\rangle|^2}{\Delta_{nm}} \tag{17}$$

is the Van Vleck susceptibility due to the transition from energy eigenstates E_n to E_m. Then

$$\Delta_{nm}=E_n-E_m \tag{18}$$

and

$$\rho_m = e^{-\beta E_m}/Z \ . \tag{19}$$

The factor $\frac{1}{2}$ in front of the Van Vleck term is due to the double counting of each transition: first by the summation over all n and m with $n \neq m$ and second by the expression $1-e^{-\beta\Delta}$. The function $P_{nm}(\hbar\omega)$ is still normalized to one [Eq. (3)] and can be a function like a Lorentzian, a Gaussian, a δ function, etc. Because of Eq. (18) $\Delta_{mm}=0$. In this case the following expression is valid:

$$\lim_{\Delta_{mm}\to 0} \frac{1-e^{-\beta\Delta_{mm}}}{\beta\Delta_{mm}} = 1 \ .$$

So Eq. (15b) becomes

$$\frac{\hbar\omega}{1-e^{-\beta\hbar\omega}} \frac{1}{\mu_B^2} \left[\sum_m \frac{\mu_B^2}{k_B T} g_J^2 \rho_m \, | \langle m \, | J_z \, | \, m \rangle |^2 \frac{1-e^{-\beta\Delta_{mm}}}{\beta\Delta_{mm}} P(Q,\hbar\omega-\Delta_{mm},T) \right.$$
$$\left. + \sum_{m\neq n} \mu_B^2 g_J^2 \rho_m \, | \langle n \, | J_z \, | \, m \rangle |^2 \frac{1-e^{-\beta\Delta_{nm}}}{\Delta_{nm}} P(Q,\hbar\omega-\Delta_{nm},T) \right] .$$

In the limit of very small linewidth and using the δ function one obtains

$$g_J^2 \sum_{m,n} \rho_m \, | \langle n \, | J_z \, | \, m \rangle |^2 \delta(\hbar\omega-\Delta_{nm}) \ . \tag{20}$$

With

$$2 \, | \langle n \, | J_z \, | \, m \rangle |^2 = | \langle n \, | J^{\perp} \, | \, m \rangle |^2$$

for cubic symmetry and using Eq. (20) instead of (15b), Eq. (6) now becomes

$$S(Q,\hbar\omega,T) = \tfrac{1}{4}(g_N r_e)^2 F^2(Q,T) g_J^2 \sum_{m,n} \rho_m \, | \langle n \, | J^{\perp} \, | \, m \rangle |^2 \delta(\hbar\omega-\Delta_{mn}) \ . \tag{6'}$$

This approximated formula is normally used for crystal-field analysis (see Brigeneau[16]).

The matrix elements and the energy levels can be obtained by diagonalization of the crystal-field Hamiltonian. For a system with a p-fold symmetry this Hamiltonian is given by

$$H_{\mathrm{CEF}} = \sum_{l>0}^{\min(2L,2J)} \sum_{m=0}^{l} B_l^m O_l^m \ , \tag{21}$$

with $l=2k$, $m=pk$; $k \in N$. Later on we shall discuss CEF effects in the tetragonal IV system $YbCu_2Si_2$. Therefore, we write down here only the formalism needed for a RE system ($L=3$) with tetragonal symmetry ($p=4$). One then has

$$H_{\mathrm{CEF}} = B_2^0 O_2^0 + B_4^0 O_4^0 + B_4^4 O_4^4 + B_6^0 O_6^0 + B_6^4 O_6^4 \ . \tag{22}$$

With the transformation of variables (similar to that used by Lea Leask and Wolf[17] in the cubic case),

$$B_2^0 = \frac{w}{3}(1-|x_1|-|x_2|-|x_3|-|x_4|), \ \sum_i |x_i| \leq 1 \ ,$$
$$B_4^0 = \frac{wx_1}{60}, \ B_4^4 = \frac{wx_2}{12}, \ B_6^0 = \frac{wx_3}{1260}, \ B_6^4 = \frac{wx_4}{60} \ , \tag{23}$$

one obtains from Eq. (22),

$$H_{\mathrm{CEF}} = W \left[(1-|x_1|-|x_2|-|x_3|-|x_4|) \frac{O_2^0}{3} + \frac{x_1 O_4^0}{60} + \frac{x_2 O_4^4}{12} + \frac{x_3 O_6^0}{1260} + \frac{x_4 O_6^4}{60} \right] . \tag{24}$$

The parameters W and x_1-x_4 must be determined by fitting the line positions and intensities of the measured inelastic neutron scattering spectra.

In normal metals, where the linewidths are determined by Ruderman-Kittel-Kasuya-Yosida (RKKY) type of magnetic relaxation and by Coulomb scattering of conduction electrons, the width of the quasielastic and inelastic neutron

TABLE I. X-ray lattice parameters of the systems studied in this paper.

System/group	Symmetry	IV system	Diamagnetic system	Magnetic system
RPd_3	cubic Cu_3Au	$CePd_3$ $a=4.213\pm0.002$ Å	$LaPd_3$ $a=4.077\pm0.006$ Å YPd_3 $a=4.235\pm0.004$ Å	$TbPd_3$ $a=4.076\pm0.005$ Å $ErPd_3$ $a=4.056\pm0.003$ Å
RBe_{13}	cubic	$CeBe_{13}$ $a=10.372\pm0.002$ Å	YBe_{13} $a=10.238\pm0.001$ Å	$TbBe_{13}$ $a=10.255\pm0.002$ Å
RSn_3	cubic Cu_3Au	$CeSn_3$ $a=4.721\pm0.003$ Å	$LaSn_3$ $a=4.7596\pm0.003$ Å	$HoSn_3$
RCu_2Si_2	tetragonal $ThCr_2Si_2$	$CeCu_2Si_2$ $a=4.103\pm0.005$ Å $c=9.94\pm0.006$ Å	YCu_2Si_2 $a=3.964\pm0.004$ Å $c=9.952\pm0.005$ Å	$TbCu_2Si_2$ $a=3.976\pm0.003$ Å $c=9.968\pm0.004$ Å
		$YbCu_2Si_2$ $a=3.927\pm0.002$ Å $c=9.997\pm0.004$ Å	$LaCu_2Si_2$ $a=4.1472\pm0.002$ Å $c=9.9137\pm0.003$ Å	
RSe	cubic NaCl	TmSe $a=5.71\pm0.004$ Å	YSe $a=5.727\pm0.004$ Å	

transition are small compared to the transition energies.[13] In intermediate-valence metals there is an additional line broadening due to the finite configurational lifetime, which affects both quasielastic and inelastic transitions and remains finite at $T\rightarrow0$. A discussion of crystal-field effects in an IV compound will be given in Sec. IV D.

III. EXPERIMENTAL PROCEDURE

The neutron scattering experiments were performed on the time-of-flight (TOF) spectrometers D7 (cold neutrons, $E_0=3.5$ meV) and the IN4 (thermal neutrons, $E_0=12.5$ meV, 51 meV) at the Institute Laue Langevin (I. L. L.) in Grenoble between 1.5 and 300 K. Additional experiments were performed on TmSe with thermal neutrons on the triple-axis spectrometer IN8 at the I. L. L. in the temperature range 2–120 K.

A schematic drawing of the TOF spectrometer D7 is shown in Fig. 1. Most of the measurements were performed on this instrument since the neutron flux at D7 is 2 orders of magnitude higher than that at IN4. The D7 spectrometer consists of a graphite monochromator, a chopper, and 32 ^{3}He detectors with collimators. The IN4 spectrometer has a double monochromator with rotating crystals taking over the function of a chopper.

The systems which were studied are listed in Table I. All systems are classified into three groups: the IV systems (with unstable $4f$ shell),

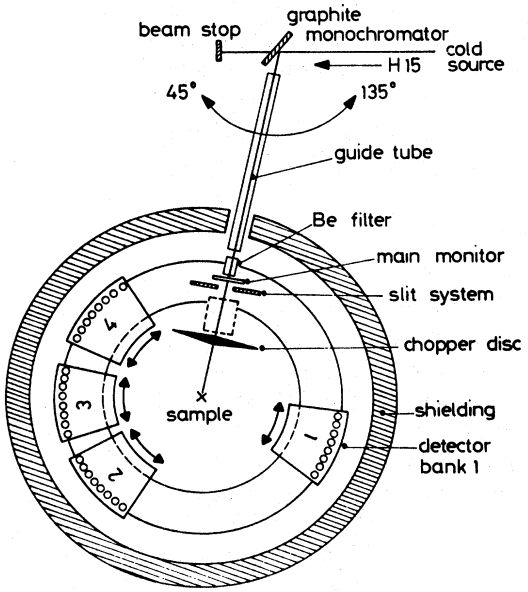

FIG. 1. Horizontal sectional drawing of the D7 spectrometer at the I. L. L. in Grenoble.

the reference systems without $4f$ electrons, and the reference systems with a stable $4f$ shell. The $R\text{Pd}_3$, $R\text{Sn}_3$, and $R\text{Cu}_2\text{Si}_2$ samples were prepared by melting the constituents together in their stoichiometric weight ratio in an argon atmosphere using a rf-induction furnace with a cold copper crucible. Weight losses were negligible (less than 0.5%) except for YbCu_2Si_2. Because of the high vapor pressure of ytterbium weight loss during melting was considerable in this compound. Therefore, ytterbium was taken with 4% initial surplus weight. The melting procedure was repeated several times until the total surplus was evaporated. The $R\text{Be}_{13}$ samples were prepared by Meyer at the University of Strassbourgh and the RSe samples by Bucher at the University of Konstanz. All samples were checked by x-ray diffraction and the resulting lattice parameters are listed in Table I.

The scattered neutron intensities measured at the detectors consists of background signal, i.e., the part scattered by the environments of the sample (sample holder, cryostat parts, etc.) and of the sample signal itself. The background signal has two parts, one absorption independent and the other absorption dependent. The absorption-dependent background scattering is that part of the environment scattering which occurs after the beam has passed the sample, i.e., it depends on the transmission of the sample. Therefore, the measurement of the empty sample holder (U_{box}) is not the correct background signal. The absorption-independent part of the background can be obtained directly by a measurement, in which the sample is replaced by a strong neutron absorber like cadmium (U_{Cd}). Then the total background signal U, which must substracted from the spectrum obtained with the sample, is given by (see Ref. 2).

$$U = U_{\text{Cd}} + T(U_{\text{box}} - U_{\text{Cd}}) , \tag{25}$$

where T is the measured transmission of the sample. For calibration of the absolute cross section a measurement of a vanadium standard was done [$\sigma^b_{\text{inc}} = 4.98$ b (Ref. 18)]. All samples were measured as powders in a flat rectangular box of aluminum.

Figure 2 illustrates various steps of the procedure adapted for data evaluation. TmSe at 120 K is used as example. Figure 2(a) shows the original TOF spectra of the sample in the aluminum box, of cadium in the box, and of the empty box. Figure 2(b) shows the spectrum of TmSe corrected for background using Eq. (25) and for energy-dependent real absorption in TmSe using the expression for an infinite plate:

$$A = 1 \frac{1/d}{(\mu(E_1)/\cos 2\theta) - \mu(E_0)} \times \frac{e^{-\mu(E_0)d} - e^{-\mu(E_1)d/\cos 2\theta}}{(e^{-\mu(E_1)d/\cos 2\theta})^{1/2}} \times (e^{-\mu(E_1)d/\cos 2\theta})^{\pm 1/2} . \tag{26}$$

with $\pm$ for $2\theta \lesssim 90°$. Here μ is the energy-dependent linear absorption coefficient, E_0 and E_1 are the energies of the incident and scattered neutrons, respectively, 2θ is the scattering angle, and d is the effective thickness of the sample. Because the absorption of thulium is rather large, the intensity in Fig. 2(b) is much larger than in Fig. 2(a). The hatched area is the elastic nuclear incoherent scattering. In the next step the spectrum is transformed from the TOF scale to the energy scale. Furthermore, the spectrum is multiplied by k_0/k_1 and corrected for the energy-dependent efficiency of the ^{3}He detectors ($A = A_0 e^{-0.56\lambda}$). In Fig. 2(c) this scattering law $\bar{S}(\theta,\hbar\omega)$ is plotted [see Eq. (1)]. The difference between $\bar{S}(\theta,\hbar\omega)$ and $S(Q,\hbar\omega)$ comes from the Q-$\hbar\omega$ dependence[14,2] for a given angle. The spectrum consists of a broad quasielastic line which has a Q dependence consistent with a magnetic form factor and the elastic incoherent scattering (hatched area). The width of the latter peak at $\hbar\omega = 0$ is given by the instrumental resolution. Dividing the magnetic scattering law by the Bose factor $1/[1-\exp(-\beta\hbar\omega)]$ one obtains the imaginary part of the dynamic susceptibility $\bar{\chi}''(\theta,\hbar\omega,T)$ [see Eq. (1)]. After further division through the local form factor $F^2(\theta) = F^2(Q,\hbar\omega)$ and β, one obtains the imaginary part of the temperature-normalized dynamic susceptibility for $Q = 0$ $\chi''(0,\hbar\omega,T)$ as shown in Fig. 2(d). The coordinate of the minimum is a direct measure of the linewidth $\Gamma/2$. Finally a division by $\hbar\omega$ leads to [see Eq. (6)]

$$\bar{R}(\theta,\hbar\omega,T) = \frac{1}{2}\left[\frac{g_N r_e}{\mu_B}\right]^2 \chi_{\text{st}}(T)\bar{P}(\theta,\hbar\omega,T) , \tag{27}$$

shown in Fig. 2(e). After correction for the form factor the functions χ'', R, and P have normally no further θ or Q dependence. Residual θ or Q dependence can, however, be expected in the linewidth at very small Q values ($Q < 0.5$ Å^{-1}).

The analysis of broad quasielastic lines is limit-

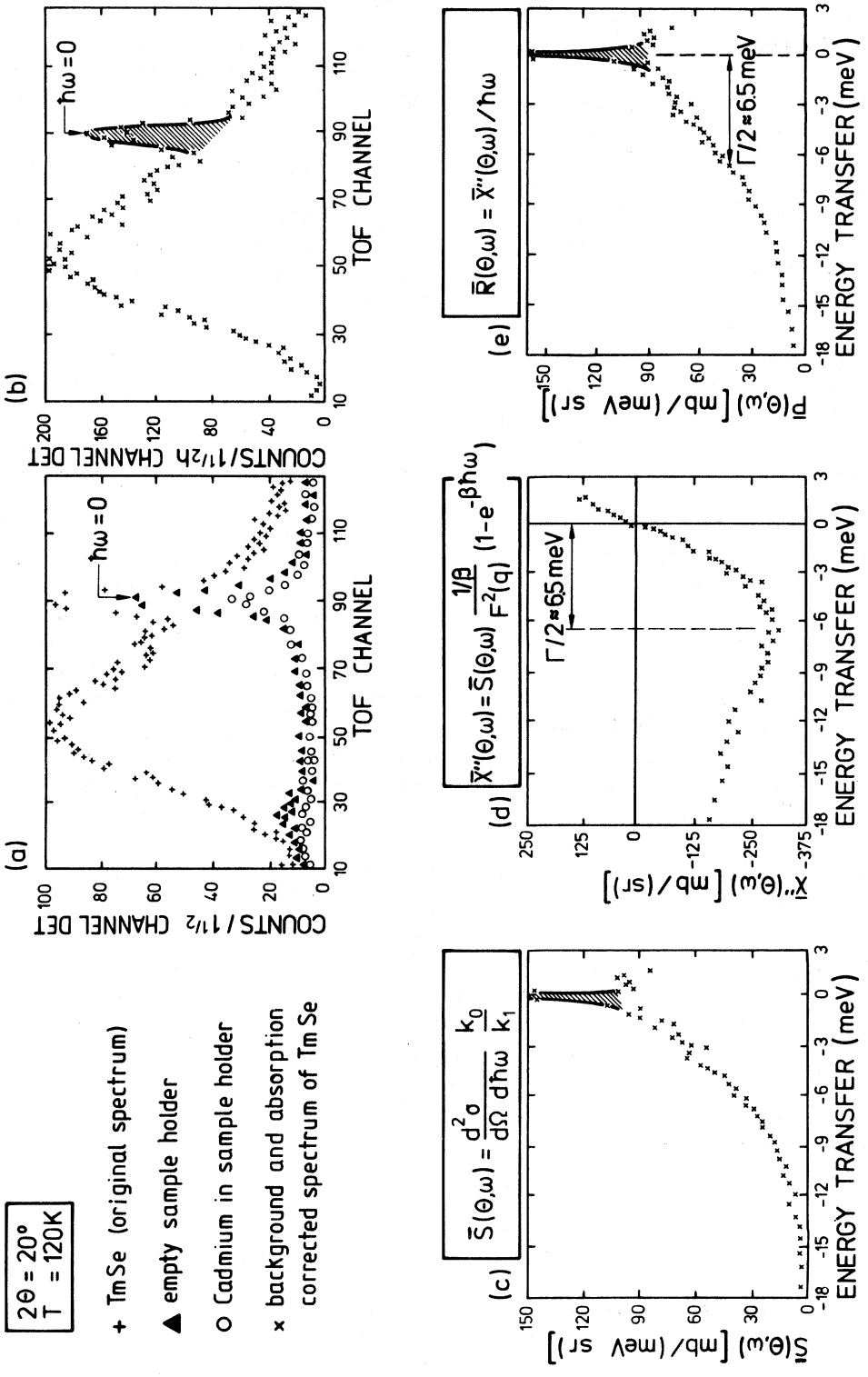

FIG. 2. Various stages of the analysis of the data to extract the quasielastic line (see text for details).

ed by two factors, namely the sample temperature and/or the incident energy of the neutrons (see Fig. 3).

(i) At $\hbar\omega < 0$ (energy gain for outgoing neutrons) the temperature is the critical point. When the thermal energy $k_B T$ becomes smaller than about $\Gamma/4$, the scattering intensity at the energy-gain side approaches the noise because of the behavior of the Bose factor.

(ii) At the energy-loss side the Bose factor is not critical since it goes to one for $T \rightarrow 0$. Here the limiting factor is the incident energy because the neutrons cannot lose more than the incident energy to the sample.

The physical reason for these two limits is obvious. On the energy-gain side the neutron can take energy from the sample of order $k_B T$ (i.e., not at $T = 0$ K), while on energy-loss side the neutron can always produce excitations in the sample with energies up to the incident energy.

IV. EXPERIMENTAL RESULTS AND DISCUSSION

A. RPd$_3$

In the RPd$_3$ intermetallic series of compounds there is at least one IV compound, CePd$_3$. We have studied this compound together with YPd$_3$ and LaPd$_3$ as diamagnetic reference compounds and TbPd$_3$ and ErPd$_3$ (Refs. 19 and 20) as representative magnetic RPd$_3$ compounds with a stable $4f$ shell. A large part of these results was reported previously.[1] All the experiments on the RPd$_3$ compounds were done on the D7 spectrometer with an incident energy of the neutrons of 3.5 meV. This incident energy turned out to be appreciably smaller than the magnetic quasielastic linewidth of CePd$_3$ ($\Gamma/2 \simeq 20$ meV). Therefore, no information about the energy dependence of the abnormal magnetic scattering in CePd$_3$ can be obtained in energy loss, and the analysis on the energy gain is restricted to temperatures of about 100 K and more because of the Bose factor (see Sec. II and Fig. 3).

Figure 4 is a modified version of Fig. 1 in Ref. 1. The analysis was improved by adding together the counts of appropriate groups of detectors at angles around 2°–20°. All three compounds show incoherent elastic scattering at $\hbar\omega = 0$ due to nuclear isotopic and/or nuclear-spin disorder. This contribution to the cross section is set apart by shading for YPd$_3$ and CePd$_3$. At finite energies the scattering in YPd$_3$ can only be due to phonons. The phonon spectrum shows intensity between -6 and -20 meV which has nearly vanished in the background at 145 K. Very little scattering is observable between -1 and -6 meV in YPd$_3$. In contrast CePd$_3$ shows considerable intensity in this window and also below the phonon peak. The integrated intensity in CePd$_3$ between -1 and -6 meV decreases with increasing Q as shown in Fig. 5. Also shown in this figure is the theoretical $4f^1$

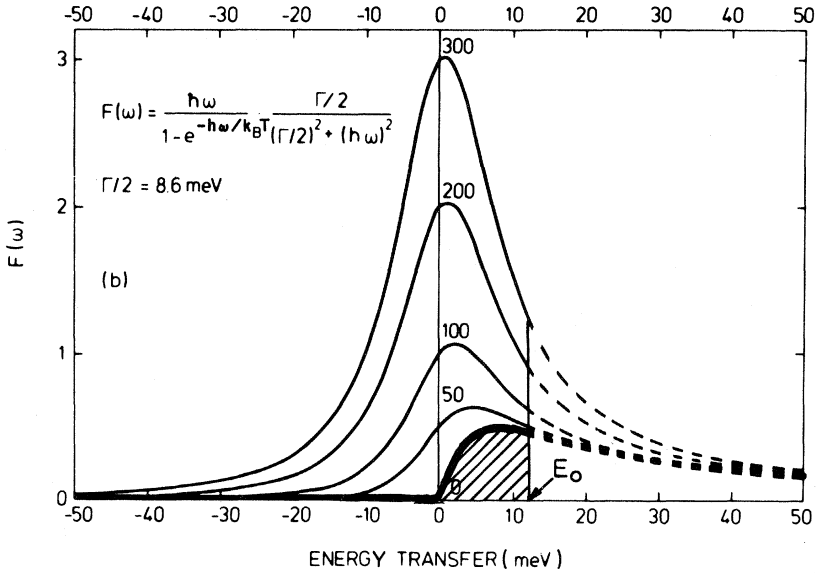

FIG. 3. Schematic drawing of the temperature dependence of the scattering cross section due to a temperature-independent quasielastic Lorentzian.

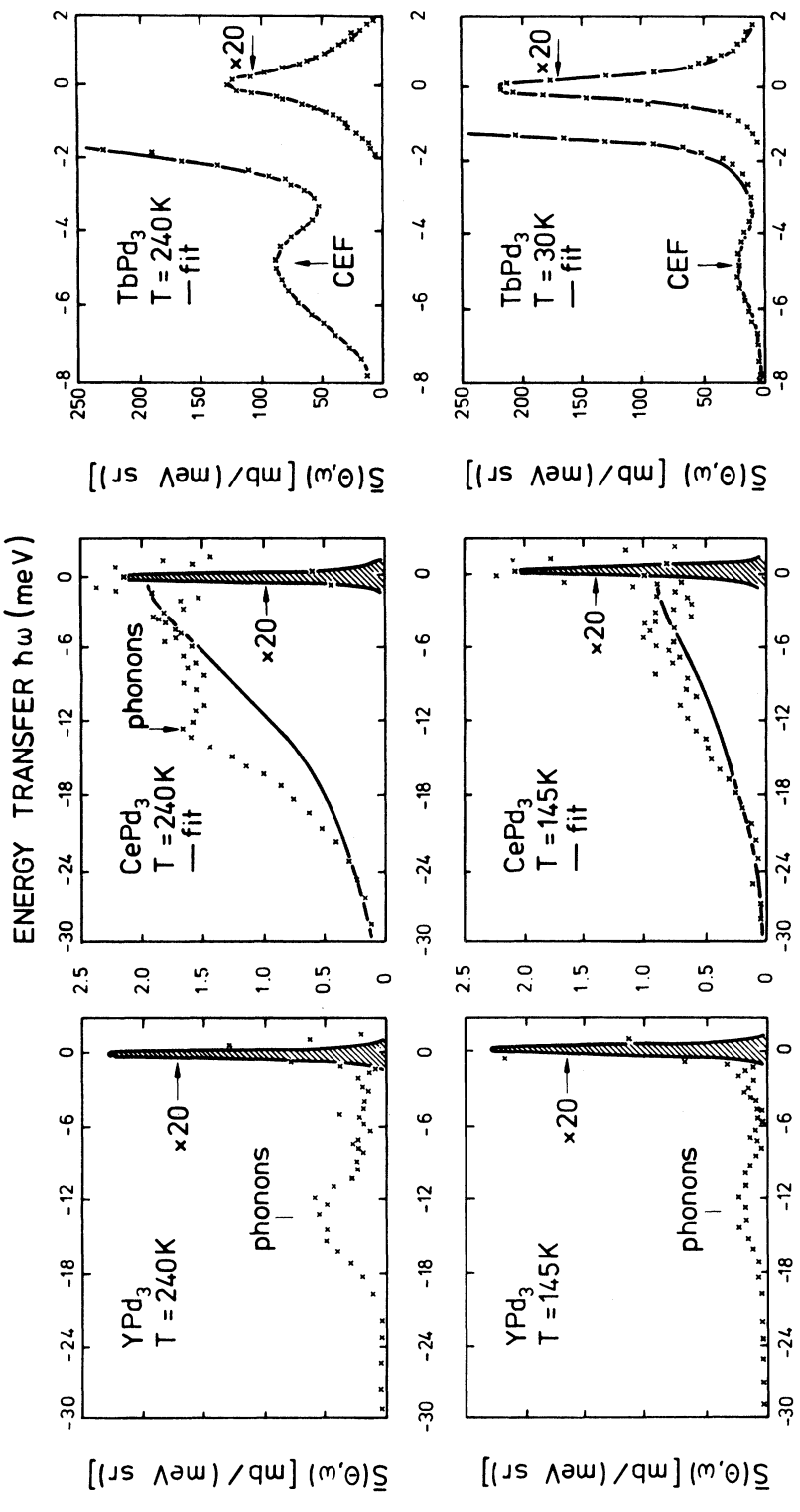

FIG. 4. Energy spectra of $CePd_3$, YPd_3, and $TbPd_3$ taken with $E_0=3.5$ meV at a constant scattering angle of $2\theta=20°$ and two different temperatures. The full line is a fit with one Lorentzian including the elastic incoherent peak.

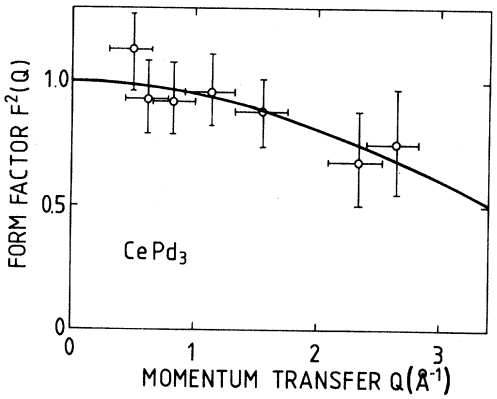

FIG. 5. Q dependence of the magnetic scattering in $CePd_3$.

form factor,[21] which is consistent with the measured Q dependence. However, the momentum transfer in our window is unfortunately not large enough to see $F^2(Q) \to 0$ for $Q \to \infty$ as, e.g., in Ce_xTh_{1-x} alloys (triple-axis spectrometer[22] or in $YbCu_2Si_2$ (TOF, to be seen later). Figure 6 shows constant Q plots of the $CePd_3$ and YPd_3 spectra at 240 K for the Q regions from 1.65 to 2.35 $Å^{-1}$ and 3.15 to 3.85 $Å^{-1}$, respectively, for averaged values of $Q=2$ and $Q=3.5$ $Å^{-1}$. Clearly at $Q=3.5$ $Å^{-1}$ the scattering is much larger than at $Q=2$ $Å^{-1}$ in both compounds, i.e., the scattering here is dominated by phonons in both cases. The lowest part of Fig. 6 results when one substracts

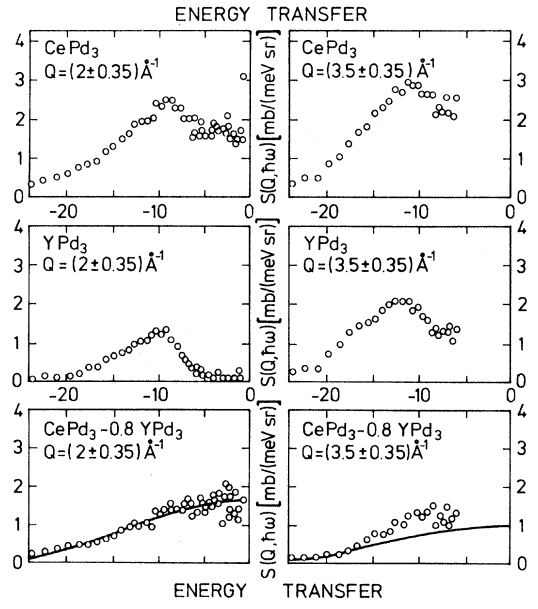

FIG. 6. Energy spectra for $CePd_3$, YPd_3, and for their difference at fixed momentum transfer Q.

the pure phonon spectrum of YPd_3 from the measured spectrum of $CePd_3$ for the same temperature and momentum transfer Q, with a correction factor of 0.8, which takes into account the different nuclear cross sections and masses of cerium and yttrium. Obviously there remains a large contribution to the neutron cross section in $CePd_3$ which decreases monotonically with increasing energy transfer and decreases only very slightly with increasing momentum transfer Q. Note that the spectrum for the larger momentum transfer (3.5 $Å^{-1}$) looks different (especially near 10 meV) from that for 2 $Å^{-1}$ even when including the modifications due to the Q dependence of the magnetic form factor (full lines). This is probably due to the simplicity of the phonon subtraction procedure, which does not consider possible changes in the phonon density of states between YPd_3 and $CePd_3$.

The neutron scattering in $TbPd_3$ is more than 1 order of magnitude stronger than in $CePd_3$. Most of the scattering is concentrated in the quasielastic line. Its maximum value increases with decreasing temperature. Its linewidth decreases accordingly, such that the integrated intensity remains nearly temperature independent. A crystal-field transition is visible at -5 meV as seen previously by Furrer and Purwins.[23] Figure 7 shows the Q dependence of the scattering in $TbPd_3$ at 240 K. The Q dependence is consistent with the theoretical $4f^8$ form factor and very close to the Q dependence of the abnormal scattering in $CePd_3$ between -1 and -6 meV. The increase of the maximum value of the quasielastic peak between 240 and 30 K is smaller than the factor 8, expected on the basis of the Korringa relation. This is partly but not entirely due to the instrumental resolution (0.3 meV) of the D7

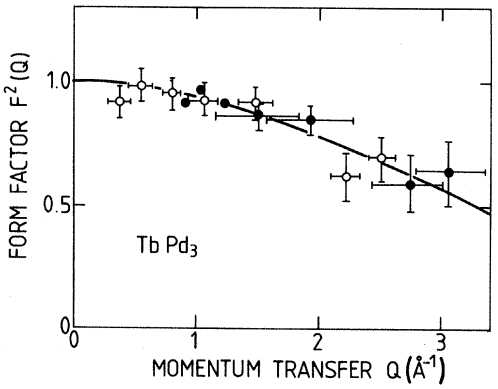

FIG. 7. Q dependence of the quasielastic scattering (○) and of the inelastic scattering around 5 meV (●) in $TbPd_3$.

spectrometer.

Figure 8 shows the temperature dependence of the quasielastic linewidth for $TbPd_3$ corrected for the experimental resoultion. This linewidth still does not extrapolate to zero for $T \rightarrow 0$ because of the existence of crystal-field transitions which cannot be resolved here, but have been detected in dilute alloys of $Tb_xY_{1-x}Pd_3$.[24] For the compound $TbPd_3$ the slope of $\Gamma/2(T)$ is about 10^{-3} meV/K (see Fig. 8) giving a Korringa coefficient $\alpha \simeq 10^{-2}$ [see Eq. (11)]. This is a very small value, but one consistent with the very small magnetic ordering temperature of $TbPd_3$, $T_N \simeq 3.9$ K.[25]

Summarizing the preliminaries we have control over the phonons via the reference compound YPd_3 and can set apart the abnormal magnetic scattering in $CePd_3$ against the normal magnetic scattering in $TbPd_3$. The Q dependence of the magnetic scattering of $TbPd_3$ and $CePd_3$ are nearly identical and indicate a well-localized $4f$ magnetization in both cases.

We now turn to the energy dependence of the magnetic scattering in $CePd_3$. In Fig. 4 the heavy lines are fits according to Eq. (6) assuming the simplest possible relaxation behavior, i.e., a Lorentzian as spectral function $P(\hbar\omega)$. For $CePd_3$ we assume a single Lorentizian as spectral function $P(Q,\hbar\omega,T)$. Such simple fits, which of course include folding with the instrumental resolution, result in numbers for two parameters: The linewidth $\Gamma/2$ and the intensity $\chi_{loc}(0,0,T)$ [see Eq. (6)]. Figure 9 shows the temperature dependence of $\Gamma/2$ thus obtained. This type of figure was the aim and is the central result of magnetic neutron scattering experiments on IV compounds. It shows that there is a drastic distinction in the magnetic relaxation of such compounds with respect to the thermally driven weak (Korringa) relaxation in RE compounds with a stable $4f$ shell (Fig. 8). While in the latter case the linewidth above the magnetic ordering temperature is of order of $10^{-2}-10^{-3}\ k_BT$, in $CePd_3$ it is about 220 K and essentially independent of temperature between 100 and 300 K. This means that the linewidth becomes arbitrarily large compared to k_BT at $T \rightarrow 0$ and is equal to k_BT at about 220 K. The relaxation time in $CePd_3$ is about 10^{-13} sec. Although we could not detect magnetic scattering below 100 K (because of the Bose factor) we can put a lower limit $\Gamma/2 > 6$ meV at 30 K.

Table II compares $\chi_{loc}(0,0,T)$ with the measured static bulk susceptibility. In their range of overlap both measurements are in agreement. This means that the static susceptibility is dominated by the contribution of the total $4f$ electrons and that other contributions, e.g., $5d\,6s$ Pauli susceptibility from conduction electrons, can only be a small fraction of the bulk static susceptibility. Equation (12), which was derived for the Curie limit ($\Gamma/2 << k_BT$), is still valid in this case too.

It is well known that cubic intermetallic compounds with cerium in a sufficiently stable $4f$ configuration show crystal-field splittings of order 10 meV. CEF splittings were also observed in the IV alloy $Ce_{0.9-x}La_xTh_{0.1}$.[26] The question arises whether such crystal-field splitting should be considered in our spectra. We expect that if there is crystal-field splitting, i.e., if the internal structure of a given configuration is preserved in the configurational motion, individual crystal-field levels should keep their relative positions but will be broadened. Therefore, if the relaxation is fast enough ($\Gamma/2 > \Delta$, Δ is the overall crystal-field

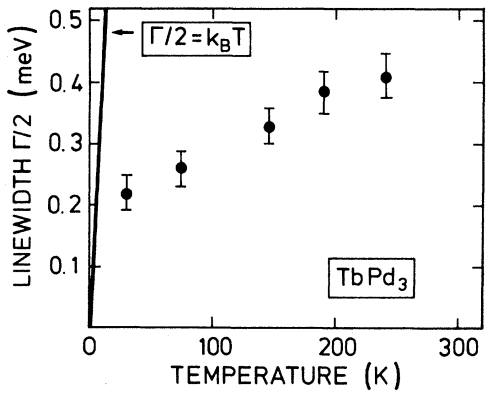

FIG. 8. Temperature dependence of the quasielastic linewidth for $TbPd_3$. The measured linewidth is small compared to the thermal energy k_BT.

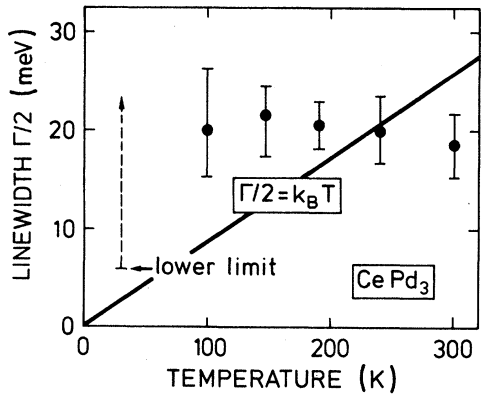

FIG. 9. Temperature dependence of the quasielastic linewidth for $CePd_3$ (single Lorentzian fits).

TABLE II. Comparison of local susceptibility obtained from neutron scattering with the bulk static susceptibility.

Sample	T (K)	$\chi_{loc}(10^{-3}$ emu/mol)	$\chi_{bulk}(10^{-3}$ emu/mol)
$CePd_3$	300	1 ±0.3	1.25
	240	1.5 ±0.2	1.39
	190	1.46±0.15	1.49
	170	1.55±0.15	1.57
$CeBe_{13}$	300	2.2 ±0.4	1.89
	220	2.34±0.3	2.23
	170	1.98±0.2	2.38

splitting), a single Lorentzian will suffice. However, in our case $\Gamma/2$ is nearly equal to the normal crystal-field splitting. The fit with a simple Lorentzian $\Gamma/2\simeq 20$ meV turns out to be identical within experimental scatter up to our limiting energy transfer to a fit where one assumes a doublet and a quartet at energy distance $\Delta=10$ meV and each multiplet with a width $\Gamma/2\simeq 13$ meV. Thus the single Lorentzian does not constitute a unique interpretation. The question arises whether some other way can be found to make a choice between the two types of spectra.

As discussed in Sec. II [Eq. (14)] the total magnetic cross section is, in principle, capable of measuring the valence. Table III shows the temperature dependence of the valence (here the fractional $4f^1$ occupation) as determined from $\chi_{loc}(0,0,T)$ assuming a Lorentzian and using cutoffs at $E_c=0.5$, 1, and 2 eV. The table contains values extracted by a fit with a single Lorentzian (columns 1, 2, and 3) and with the above crystal-field spectrum (columns 4, 5, and 6). Note that while the fits with and without crystal fields are coincident within experimental error and in the measured energy-transfer range, the total cross sections come out different. The reason is that with crystal fields the linewidths are smaller than without so that the extrapolation of the spectrum beyond our limiting energy transfer contains more intensity without than with crystal fields. The

TABLE III. Valence extracted from various experimental methods (see text). E_c is the cutoff energy for the intergation (Eq. 14).

		$4f$ occupation number								
		Neutron scattering						Lattice parameter		L_{III} edge
Compound	T	without CEF			with CEF					
	(K)	$E_c=0.5$ eV	$E_c=1$ eV	$E_c=2$ eV	$E_c=0.5$ eV	$E_c=1$ eV	$E_c=2$ eV			
$CePd_3$	300	0.63	0.7	0.77	0.6	0.66	0.72	0.55	0.775	0.77
	240	0.62	0.7	0.79	0.59	0.65	0.73	0.52	0.76	
	190	0.62	0.71	0.81	0.57	0.65	0.74	0.49	0.745	
	145	0.62	0.73	0.84	0.57	0.66	0.75	0.47	0.735	
	100	0.55	0.64	0.75	0.48	0.56	0.65	0.45	0.725	
	23									0.71
$CeBe_{13}$	300	0.93	1.15	1.29	0.89	1.08	1.2	0.8	0.9	>0.9
	220	0.94	1.18	1.34	0.89	1.08	1.22	0.76	0.88	
	170	0.98	1.17	1.36	0.9	1.07	1.22	0.71	0.855	
	120	0.98	1.08	1.27	0.87	0.95	1.1	0.67	0.835	
$CeSn_3$	300	1.01	1.03	1.12	0.97	0.98	1.06	0.9	0.95	>0.9
	220	1	1.07	1.2	0.94	1.0	1.11	0.88	0.94	
	170	0.99	1.15	1.32	0.91	1.05	1.19	0.84	0.92	
	120	0.89	1.18	1.39	0.8	1.04	1.21	0.8	0.9	
Column		1	2	3	4	5	6	7	8	9

values obtained with crystal-field spectra are in better agreement with values obtained by other methods, e.g., with the valence extracted from lattice parameters[27–29] using the usual interpolation (column 7) or using the model discussed in Ref. 30 (column 8) or the valence measured directly by the L_{III} x-ray absorption edge[30] (column 9). We see that not only the choice of spectrum but also that of the cutoff affects the value of the valence. We cannot justify any of the cutoffs on the basis of neutron scattering alone. Thus Table III should only be viewed to offer some stones to the mosaic of valence determinations through different experimental methods. It seems that only via such a mosaic one can finally arrive at reliable values for the valence of IV compounds.

B. RBe$_{13}$

Figure 10 shows the energy spectra of $CeBe_{13}$, YBe_{13}, and the difference spectrum at 300 K. The main phonon contribution in this compound comes at very high frequency (above 25 meV), mainly because of the small mass of the beryllium. This allows to extract the magnetic scattering near $\hbar\omega=0$ without any problems. Figure 11 shows the linewidth as function of temperature as extracted from such data under the assumption of a single Lorentzian. Table II shows again a comparison between the static bulk susceptibility $\chi_{st}(T)$ (Ref. 31) and $\chi_{loc}(0,0,T)$ as extracted here. Again as in $CePd_3$ the agreement is quite satisfactory, i.e., the static bulk susceptibility is dominated by the local $4f$ magnetization. Table III shows again the valence as a function of temperature obtained from these data by various methods of analysis.

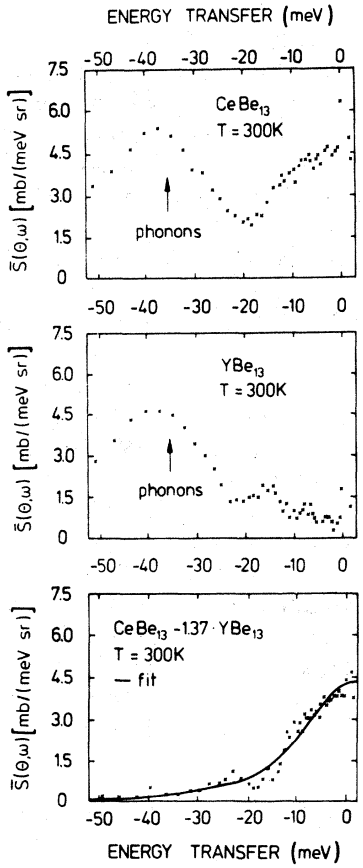

FIG. 10. Energy spectra of $CeBe_{13}$, YBe_{13}, and of their difference taken with $E_0=3.5$ meV at a scattering angle of $2\theta=20°$ and at room temperature. The full line is a single Lorentzian fit.

C. RSn$_3$

Figure 12 shows the energy spectra of $CeSn_3$, $LaSn_3$, and the difference spectrum at 300 K. Note that the phonons in the RSn_3, are very much softer than in the RPd_3 so that the best window for magnetic scattering is above -20 meV. Obviously the proper phonon subtraction procedure is much more important here. As in RPd_3 the measurements were performed with cold neutrons (D7) and therefore no sufficiently accurate numbers can be obtained for $\Gamma/2$ below 100 K. The linewidth as a function of temperature is shown in Fig. 13. Since the phonons dominate the spectrum between 0 and -20 meV it was not possible to independently extract $\chi_{loc}(0,0,T)$ and $\Gamma/2(T)$ from the neutron scattering data alone with sufficient accuracy. We therefore used $\chi(0,0,T)$ from the static bulk susceptibility to obtain the values of $\Gamma/2$ shown in Fig. 13. This procedure seems justified

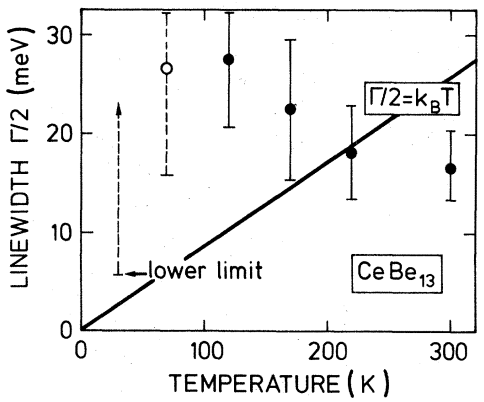

FIG. 11. Temperature dependence of the quasielastic linewidth for $CeBe_{13}$ (single Lorentzian fit). The point at $T=70$ K is open because of its large uncertainty.

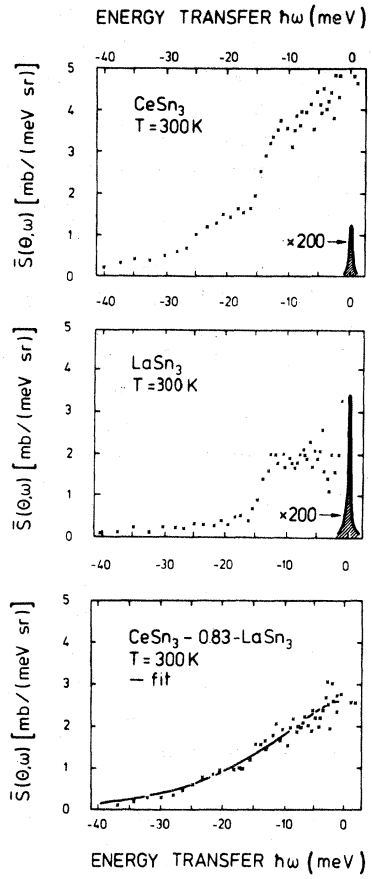

FIG. 12. Energy spectra of $CeSn_3$, $LaSn_3$, and of their difference taken with $E_0=3.5$ meV at a scattering angle of $2\theta=20°$ and at room temperature. The full line is a single Lorentzian fit.

in view of the agreement between the bulk susceptibility and the independently determined $\chi_{loc}(0,0,T)$ from neutron scattering data alone in the case of $CePd_3$ and $CeBe_{13}$. Table III again

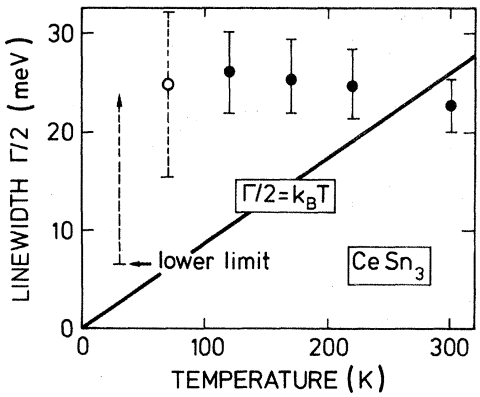

FIG. 13. Temperature dependence of the quasielastic linewidth for $CeSn_3$ (single Lorentzian fit). The point at $T=70$ K is open because of its large uncertainty.

shows the valence as a function of temperature obtained by various methods of analysis.

D. RCu_2Si_2

In Ref. 3 we reported data on diffuse magnetic neutron scattering as function of temperature on $YbCu_2Si_2$, with $LaCu_2Si_2$ as a reference. The main result of this paper was the clear proof of the existence of a finite width $\Gamma/2$ if the quasielastic line at thermal energies $k_BT << \Gamma/2$. This result, which in the meantime was also obtained for YbCuAl,[32] is very important because it shows that the quasielastic line of finite width is a property of the ground state and not due to the thermal relaxation. In order to obtain this type of result one needs to measure at sufficient low temperature ($k_BT << \Gamma/2$). Because of the Bose factor this implies that one cannot measure in energy gain and that the measurements must be done on the energy-loss side with an incoming neutron energy $E_0 > \Gamma/2$. Since all measurements on Ce compounds reported in Secs. IV A–IV C were done on D7 with an incoming energy of about 3.5 meV (an energy small compared to the linewidth found in these experiments), it was not possible to establish there the existence of fast relaxation in the limit $k_BT << \Gamma/2$. The measurements on $YbCu_2Si_2$ reported in Ref. 3 were done on the IN4 spectrometer with an incoming energy $E_0=12.5$ meV, somewhat larger than the width $\Gamma/2 \simeq 6$ meV found at $T=5$ K (see Fig. 3). In order to check whether there are inelastic lines due to residual crystal-field transitions at higher energy transfer we have extended the measurements on $YbCu_2Si_2$ to an incoming energy of about 51 meV (IN4). In the following we report on measurements with all three incoming energies at temperatures between 5 and 300 K. The emphasis will be on an evaluation of the measurements with 51 meV, since they give clearest information of crystal-field effects. The analysis will be done in three steps: Separation of phonon and magnetic scattering, extraction of the magnetic form factor, and analysis of the energy dependence of the magnetic scattering.

1. *Separation of magnetic and phonon scattering*

Figures 14 and 15 show the energy dependence of the neutron cross section at small and large scattering angles (2θ = 17°,69°) for $LaCu_2Si_2$ and $YbCu_2Si_2$, respectively, at $T=250$ K and $E_0=51$

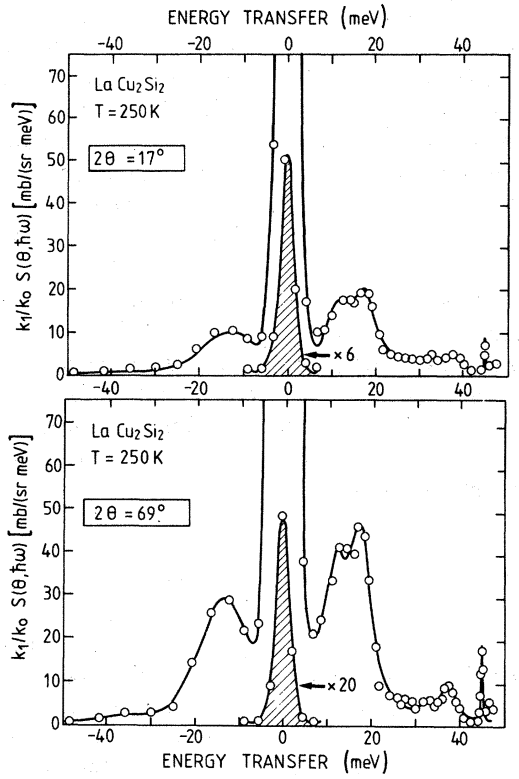

FIG. 14. Energy spectra of $LaCu_2Si_2$ taken with $E_0=51.5$ meV at $T=250$ K for two different scattering angles.

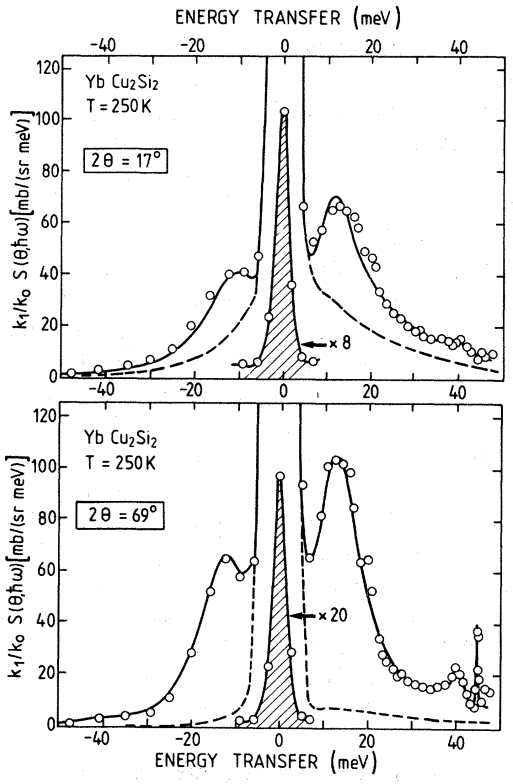

FIG. 15. Energy spectra of $YbCu_2Si_2$ taken with $E_0=51.5$ meV at $T=250$ K for two different scattering angles. The full line is a complete fit (phonon plus magnetic). The dashed line is a single Lorentzian fit of the magnetic part.

meV. For $LaCu_2Si_2$ we observe the usual elastic incoherent scattering peak (hatched area) and phonon scattering at finite $\hbar\omega$ with maximum intensity at 10 and 15 meV. Positions and intensities of the several phonon peaks are listed in Table IV taken from fits shown in Figs. 14 and 15 by the drawn-out lines. Note that the ratio of the low phonon energy of $YbCu_2Si_2$ and the average value of the two low phonon energies of $LaCu_2Si_2$ is equal to the square root of mass ratio $\sqrt{M_{La}/M_{Yb}}$, i.e., this phonon contribution is mainly due to RE atoms. Furthermore, in the previous analysis of the data taken on the IN4 with an incident energy of 12.5 meV (Ref. 3) we had no

TABLE IV. Fit results for the phonons in $YbCu_2Si_2$ and $LaCu_2Si_2$ at $T=250$ K.

Sample		$2\theta=17°$			$2\theta=69°$		
		Δ (meV)	Γ/2 (meV)	I (b)	Δ (meV)	Γ/2 (meV)	I (b)
$LaCu_2Si_2$	1	11.2	2.8	0.71	11.6	2.4	1.52
	2	17.2	2.8	1.02	17.3	2.4	2.38
	3	32.7	2.83	0.25	32.2	1.3	0.48
	4	37.7	1.3	0.15	37.3	1.9	0.57
	5	45	0.09	0.03	45	0.1	0.27
$YbCu_2Si_2$	1						
	2	12.8	6.0	4.97	12.8	5.3	9.9
	3	37.2	2.2	0.22	36.7	1.7	0.23
	4	40.25	2.2	0.26	40.27	1.7	0.88
	5	44.9	0.04	0.036	44.9	0.05	0.37

problems with phonon scattering, because in this experimental setup we could only measure up to an energy loss of about 10 meV, i.e., in this case we did not see any phonon scattering. For the experiment with $E_0=51.5$ meV we have plotted the scattering intensity around 13 meV against momentum transfer Q for angles between 8° and 140° in a double logarithmic plot for both $LaCu_2Si_2$ and $YbCu_2Si_2$ at 250 K in Fig. 16. The horizontial error bars arise from the fact that the counts of (maximally) four detectors around the chosen angle and the counts in a main phonon energy window 8–18 meV wide were added up in order to reduce the noise. For both substances one can distinguish between a high and a low Q region. For both regions one obtains a cross section $\sigma(Q)=CQ^n$, however, with different exponents for $LaCu_2Si_2$, $n\simeq 0.5$ for $Q<5$ Å^{-1} and $n\simeq 1.95$ for $Q>5$ Å^{-1}. The last exponent is near the expected value of 2 for the Q dependence of phonon scattering. We do not know why the exponent n at small Q has unexpectedly a smaller value. This cannot be due to simple background effects; perhaps multiple-scattering processes can be the reason. For $YbCu_2Si_2$ the scattering intensity is nearly Q independent at small Q. At high Q, however, the plot goes asymptotically against $\sigma(Q)=CQ^n$ with again $n\simeq 2$. Therefore, one can be quite sure that phonon scattering is dominant in both compounds at large Q. The ratio $C(\mathrm{Yb})/C(\mathrm{La})=\sigma(\mathrm{Yb})/\sigma(\mathrm{La})\simeq 2.4$ extracted at large Q is close to the one expected from the different nuclear cross sections of ytterbium and lanthanum which for identical phonon spectra should be 2.3 assuming a vibration of the RE atoms only. However, the detailed values of this ratio depend also on differences of the phonon spectra about which we have no further information. The factor $C(\mathrm{Yb})/C(\mathrm{La})$ as determined here was used later in the separation of magnetic from phonon scattering at various incoming energies, energy transfers, and temperatures. For small Q values, however, the ratio $\sigma(\mathrm{Yb})/\sigma(\mathrm{La})$ goes to a value of about 4.5. This additional scattering intensity of $YbCu_2Si_2$ must be due to magnetic scattering.

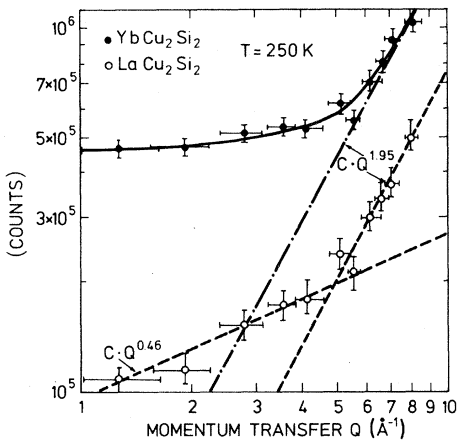

FIG. 16. Double logarithmic plots of the scattering intensity in the energy window 8–23 meV (energy gain) vs momentum transfer from the spectra of $YbCu_2Si_2$ and $LaCu_2Si_2$ at $T=250$ K. The full line is a guide to the eye. The dashed line shows the behavior of $LaCu_2Si_2$ and the dashed-dotted line the extrapolated behavior ($Q\rightarrow\infty$) for $YbCu_2Si_2$.

2. *Magnetic form factor*

Figure 17 shows the magnetic form factor extracted from the scattering cross section of $YbCu_2Si_2$ after subtracting the phonon contribution. The data were taken with an incoming energy of 51 meV. The drawn-out line is the theoretical $4f^{13}$ form factor.[21] The agreement of our experimental points with the theoretical form factor out to the highest Q values, where the magnetic scattering vanishes, is very satisfactory. The data were actually taken in an energy window, where the phonon intensity is largest. The good agreement of the magnetic contribution with the theoretical $4f$ form factor therefore is an indication for the reliability of the phonon subtraction procedure.

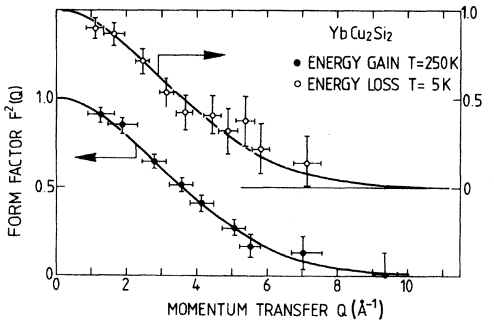

FIG. 17. Q dependence of the scattering intensity of the difference spectrum $[YbCu_2Si_2]-2.4[LaCu_2Si_2]$ for the same energy window as in Fig. 16. The experimental points agree quite well with the theoretical $4f^{13}$ form factor.

3. *Energy dependence of the magnetic scattering*

In a first step the energy-dependence magnetic scattering was extracted at low Q from the data of $YbCu_2Si_2$ taken with 51-meV incoming energy by subtracting of the energy-dependent phonon contribution of $LaCu_2Si_2$ multiplied by the factor $C(Yb)/C(La)$. Such spectra show a smooth energy dependence superimposed by sharp peaks and dips at positions of the phonons in $LaCu_2Si_2$. These sharp structures are obviously due to small shifts of the phonon peaks in $YbCu_2Si_2$ with respect to those in $LaCu_2Si_2$. In the next step one quasielastic line of Lorentzian shape was fitted through the difference spectrum. This fit (including the elastic line) is shown in Fig. 15 (dashed line). The difference between the fit of the difference spectrum and the measured spectrum represents now the phonon scattering distribution of $YbCu_2Si_2$.

The quasielastic linewidths for all three experiments ($E_0=3.5$, 12.5, and 51.5 meV) obtained with single Lorentzian fits are plotted versus temperature in the upper part of Fig. 18. The magnetic cross section [$\Sigma_{loc} \propto \chi_{loc} T$; see Eq. (12)] obtained from these single-line Lorentzian fits (e.g., Fig. 15, dashed line) are listed in Table V for the data taken with $E_0=51.5$ meV. There are two problems with such single-line fits: First the quasielastic linewidth obtained from the data taken with $E_0=51.5$ meV strongly differs from those taken with $E_0=3.5$ meV (Fig. 18, upper part). Second, the cross section from the data taken with $E_0=51.5$ meV at temperatures above T_{SF} is 2 times larger than expected from a broadened set of eight Hund's-rule ground-state Zeeman levels (trivalent ytterbium, see Table V). In short, single-line fits do not yield consistent results from measurements with different incoming energies. Here, therefore, the question clearly arises whether single-line fits are appropriate.

The magnetic cross section is obtained by integrating the Lorentzian from minus to plus infinity. It turns out that for single-line fits such as those with $E_0=51.5$ meV more than half of the total intensity comes from an energy range which is inaccessible to experiment, i.e., a considerable part of this number is based on an *extrapolation* to high-energy transfer. The fact that the cross section of a single Lorentzian comes out to be twice too large is then a clear indication that we are extrapolating the wrong curve. Let us assume that the spectrum consists not just of a single quasielastic line, but of a quasielastic and an inelastic line, the latter centered at an energy comparable to or smaller than the width of both lines. The inelastic line would then not manifest itself by a separate peak and the spectrum could be mistaken for a single-line spectrum with a total width $\Gamma/2$. However, the width of either line ($\Gamma_1/2$,$\Gamma_2/2$) would then be smaller than $\Gamma/2$. If one then compares the cross sections of both fits (one of the single line with $\Gamma/2$, the other with two lines $\Gamma_1/2$, $\Gamma_2/2$ $<\Gamma/2$), the cross section of the single line will come out larger than that of the double-line spectrum.

The fact that the quasielastic linewidth at low temperatures extracted from the data with $E_0=51.5$ meV is much larger than that extracted

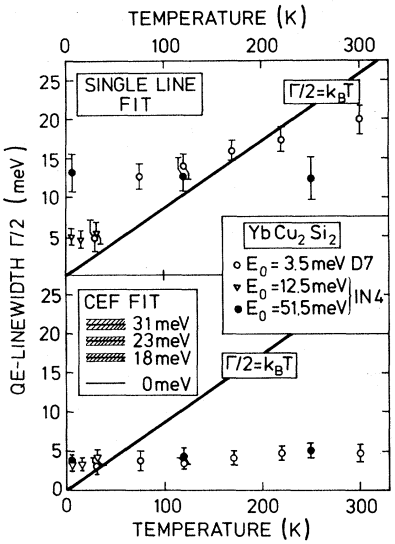

FIG. 18. Temperature dependence of the quasielastic linewidth $\Gamma/2$ for $YbCu_2Si_2$. The upper part shows the results of single Lorentzian fits, while the lower part shows the results of the fits with the crystal-field scheme shown in the inset of the lower part.

TABLE V. Local magnetic cross section of $YbCu_2Si_2$ obtained from single Lorentzian fits. Note that because of $\Sigma_{loc}=\chi_{loc}T$ and the nearly temperature-independent static susceptibility at low temperatures, Σ_{loc} decreases for decreasing temperatures. As a comparison the local magnetic cross section of a free Yb^{3+} ion is given.

T (K)	250	120	5
Σ_{loc} (b)	24.5	17.7	0.95
$\Sigma_{loc}(Yb^{3+})$ (b)	12.54	12.54	12.54

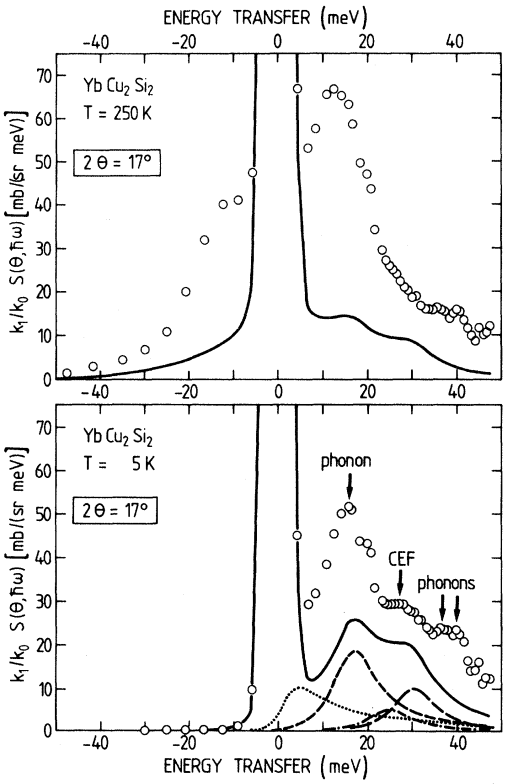

FIG. 19. Energy spectra of $YbCu_2Si_2$ taken with $E_0=51.5$ meV at a scattering angle of 17° for $T=250$ and 5 K. The full line is the magnetic spectrum obtained from a complete fit (magnetic and phonon) shown in Fig. 15. In the low-temperature spectrum the quasielastic (dotted line) and the three inelastic excitation lines (dashed lines) are shown separately.

from the data with $E_0=3.5$ meV can also be explained in a picture of several lines. Let us assume a multiline spectrum for high temperatures. One then observes a mixture of quasielastic and inelastic lines with both thermal (51.5 meV) and cold (3.5 meV) neutrons. At low temperatures an inelastic line at about 20 meV is only detectable with thermal neutrons, not with cold neutrons. Therefore, at low temperatures and with cold neutrons one can only observe the quasielastic line resulting in a less broad spectrum compared to high temperatures, while at low temperatures with thermal neutrons one still observes a mixture of quasielastic and inelastic scattering, i.e., a broad spectrum even at low temperatures.

These two problems tell us that we are dealing with a multiline spectrum rather than with a single quasielastic line. Apparently the widths of all these lines are so large that it is difficult to distinguish a magnetic line individually. Only the low-temperature spectrum of $YbCu_2Si_2$ ($T=5$ K) in Fig. 19 shows, in comparison with the spectrum at $T=250$ K, a direct indication for a magnetic excitation at about 31 meV. There are two reasons for this statement. Firstly, there is no peak visible in the energy range from 23–35 meV at high temperatures and large Q values (see Fig. 15, lower part). Secondly, the scattering intensity in this energy range increases with decreasing temperature, which is typical for a magnetic excitation starting from the ground state but is in contrast to phonon scattering.

The most natural cause for a magnetic multiline spectrum is of course crystal-field splitting. In tetragonal RCu_2Si_2 compounds the CEF splittings are in fact rather large, larger than in cubic symmetry. In $CeCu_2Si_2$ for instance an overall splitting of 31 meV was found by inelastic neutron scattering.[33] Moreover the anisotropy of the static susceptibility of single crystals[34] proves that CEF effects must survive the valence fluctuation in $YbCu_2Si_2$.

The data published earlier[3] ($E_0=3.5$ and 12.5 meV) were already analyzed with a multiline spectrum, namely one quasielastic and one inelastic line. However, the new data with $E_0=51.5$ meV do not yet fit this spectrum consistently. Thus all data had to be reanalyzed.

In a tetragonal crystal field the $J=\frac{7}{2}$ Hund's-rule ground state will split into four doublets. Line positions and transition probabilities are defined by five independent crystal-field parameters (see Sec. II D). Obviously it is difficult to obtain a unique set of parameters from fits to spectra which do not even show individual lines because of their large broadening. We have assumed that all levels have the same width (quasielastic linewidth) and that for the transitions the linewidths are larger by a factor of 1.35. Moreover we have required consistency of the analysis for the data of the three incoming energies and that the cross section be that expected from the static susceptibility. In a sense therefore the fits can be said to yield five parameters on a basis of four independent measurements. The analysis yields two most likely sets of CEF parameters, namely either $W=2.5\pm0.3$ meV, $x_1=-0.41\pm0.1$, $x_2=0.07\pm0.05$, $x_3=0.15\pm0.05$, $x_4=0.13\pm0.05$, or $W=-2.5\pm0.3$ meV, $x_1=0.41\pm0.1$, $x_2=-0.08\pm0.05$, $x_3=0.15\pm0.05$, or $x_4=0.12\pm0.05$. Both versions have an approximate energy-level sequence of 0–18–23–31 meV (see inset of Fig. 18, lower part). The hatched areas indicate the errors for the positions of the en-

ergy levels. The lower part of Fig. 18 shows the quasielastic linewidth versus temperature extracted from all three experiments. This linewidth is nearly temperature independent and coincides within scatter for all three experiments. The decrease of the linewidth from the upper to the lower part of Fig. 18 is rather dramatic. It demonstrates that reliable linewidths can only be obtained from a rather volumious set of data taken at different incoming energies. Where such work has not been done (e.g., Figs. 9, 11, and 13 for Ce compounds) the numbers given for the linewidths should only be taken as upper limits.

E. TmSe

TmSe has a special status among the IV compounds since it orders antiferromagnetically at $T_N \simeq 3.5$ K. Most of the inelastic neutron scattering data have been shown and discussed in several earlier papers.[4,35,36] Here we wish to mention a feature of the data which seems quite significant to us, but was heretofore not yet mentioned in the literature. The main and well-known features of TmSe are the following: At temperatures above 100 K the spectrum looks like a single quasielastic line with $\Gamma/2 \simeq 6.5$ meV, while below 100 K it splits into an inelastic and a quasielastic line. The position of the inelastic line shifts from 6 meV at 60 K to 10 meV at 10 K (see Fig. 20; squares), where it has a width of about 2 meV. The width of the quasielastic line decreases linearly with temperatures below 100 K with $\Gamma/2 \simeq k_B T$. At 3.5 K the width then is sufficiently low to admit magnetic order at a temperature which is quite in line with that of magnetically stable Tm compounds, e.g., TmS.

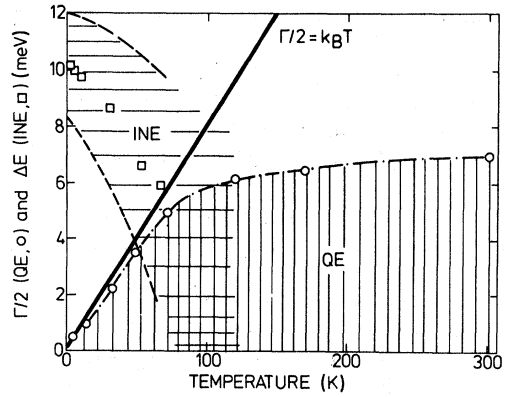

FIG. 20. Temperature dependence of the quasielastic linewidth (○) and of the position of the inelastic line (□) in TmSe.

The important and yet unmentioned point is that if one tries to extract $\chi_{st}(T)$ from the local magnetic cross section Σ_{loc} using Eq. (12) one does not reproduce the measured static susceptibility of TmSe. This procedure on the other hand has so far resulted in good agreement between neutron data and susceptiblity in all other IV compounds. If one, however, uses Eq. (13) with $\Theta = -50$ K one finds good agreement between the local magnetic cross section and the bulk susceptibilities in TmSe too: The local magnetic moment extracted from the neutron data and the effective moment from the high-tempetature susceptibility are then identical within the experimental error [$\mu_{eff} = (6.32 \pm 0.1)\mu_B$].

As discussed in Sec. II, Eq. (13) must be applied if the form factor at $Q \to 0$ is different from the fully local $4f$ form factor, i.e., if there are magnetic correlations between RE sites. Apparently in TmSe some type of effective antiferromagnetic interaction is present which decreases the $Q \to 0$ form factor with decreasing temperature away from the local value. TmSe is the only known IV system in which any such magnetic correlation effects have been observed so far. These correlations apparently exist at room temperature. We wish to point out that the energy of that correlation ($\Theta = -50$ K) cannot be due to simple RKKY interaction, whose energy is more than 1 order of magnitude smaller (scaling the spin interaction of TbSe to TmSe via the de Gennes factor one arrives at a RKKY energy of about 5 K which agrees reasonable well with the measured Neél temperature).

V. CONCLUSION

In this paper we have presented the detailed analysis of the energy and momentum dependence of the neutron scattering cross section of several IV compounds. In all compounds we find within the limited experimental resolution a completely normal spatial distribution of the $4f$ orbital and spin magnetization, i.e., the local $4f$ form factor without any magnetic correlations between RE sites strong enough to be detectable, except TmSe. (Measurements with a higher resolving method have found an abnormal form factor in $CeSn_3$ at low temperatures.[37]) On the other hand the energy dependence of this magnetic scattering was found to be abnormal in every case. The anomaly con-

sists in a wide spread in energy without any outstanding features like crystal-field transitions. In first approximation the energy dependence can be viewed as a nearly temperature-independent quasielastic Lorentzian distribution in all cases except for TmSe at low temperatures. However, in some cases ($YbCu_2Si_2$) the quasielastic linewidth thus obtained depends on the incoming energy of the neutron at a fixed temperature (see Fig. 18, upper part). This together with certain problems with the total magnetic cross section leads to the inescapable conclusion that such a spectrum consists not of a single quasielastic line but of one quasielastic and several inelastic lines, each with a smaller width than the above single Lorentzian. We interpret such multiline spectra as strongly broadended crystal-field spectra. The CEF transition lines cannot be distinguished directly in the spectrum. There are several such multiline spectra which fit the data even under the restrictions given by the crystal-field symmetry. In the compounds other than $YbCu_2Si_2$ the neutron data can be interpreted with a single-line or with a multiline CEF spectrum; the neutron experiment cannot distinguish between these possibilities.

Recent theories[11,38,39] try to establish correlations between neutron quasielastic line and the characteristic temperature which appears in the temperature dependence of the static susceptibility. The theory of Kuramoto and Müller-Hartmann[11] also connects the magnetic linewidth directly with the valence. We wish to point out that since the individual linewidth of multiline spectra are smaller than that of the single-line analysis used in Figs. 9, 11, and 13 and elsewhere[1-5,32] and since all spectra probably have an underlying multiline (CEF) structure, the numbers from those figures are very likely overestimates of the true linewidth. The only reasonably final linewidths in this paper are those of $YbCu_2Si_2$. This fact must be borne in mind when comparing theory with our experiment. There are other data which after careful analysis can distinguish between single and multiline CEF spectra, namely those which measure the temperature dependence of the valence via x-ray diffraction,[40] capacitive thermal expansion,[41,42] or L_{III} x-ray absorption.[43] Future interpretation of the neutron scattering spectra will have to be consistent with their analysis.

ACKNOWLEDGMENTS

We thank W. Schmatz for his strong support of this research at the Kernforschungsanlage Jülich, and H. Scheuer, W. Just, and J. B. Suck for their help during the experiments at the I. L. L. Grenoble, S. Horn for his help in the crystal-field analysis, M. Beyss for advice during the sample preparation, A. Meyer and E. Bucher for their providing samples of $R\mathrm{Be}_{13}$ and $R\mathrm{Se}$, respectively, and E. Müller-Hartmann, Y. Kuramoto, A. Bringer, and H. Lustfeld for their theoretical discussions. This work was supported by the Deutsche Forschungsgemeinschaft through Sonderforschungsbereich SFB 125.

[1]E. Holland-Moritz, M. Loewenhaupt, W. Schmatz, and D. Wohlleben, Phys. Rev. Lett. 38, 983 (1977).
[2]E. Holland-Moritz, Dissertation, University of Cologne, 1978 (unpublished), appearing in reports of the Kernforschungsanlage Jülich, Jül-Spez 14 (1978).
[3]E. Holland-Moritz, D. Wohlleben, and M. Loewenhaupt, J. Phys. (Paris) 39, C6-835 (1978).
[4]M. Loewenhaupt and E. Holland-Moritz, J. Appl. Phys. 50, 7456 (1979).
[5]M. Loewenhaupt and E. Holland-Moritz, J. Magn. Magn. Mater. 14, 227 (1979).
[6]E. E. Vainshtein, S. M. Blokhin, and Y. B. Paderno, Fiz. Tverd. Tela. (Leningrad) 6, 2909 (1965) [Sov. Phys—Solid State 6, 2318 (1965)].
[7]J. N. Chazalviel, M. Campagna, G. K. Wertheim, and P. Schmidt, Solid State Commun. 19, 725 (1976).
[8]R. L. Cohen, M. Eibschütz, and K. W. West, Phys. Rev. Lett. 24, 383 (1970).
[9]G. E. T. Gonçalves da Silva and L. M. Falicov, Phys. Rev. B 13, 3948 (1976).
[10]L. L. Hirst, Phys. Rev. B 15, 1 (1977).
[11]Y. Kuramoto and E. Müller-Hartmann, in *Valence Fluctuations in Solids*, edited by L. M. Falicov, W. Hanke, and M. B. Maple (North-Holland, New York, 1981).
[12]J. Korringa, Physica (Utrecht) 16, 601 (1950).
[13]K. W. Becker, P. Fulde, and J. Keller, Z. Phys. B 28, 9 (1977).
[14]W. Marshall and S. W. Lovesey, *Theory of Thermal Neutron Scattering* (Clarendon, Oxford, 1971).
[15]R. M. White, *Quantum Theory of Magnetism* (McGraw-Hill, New York, 1970).
[16]For example, R. J. Birgenau, J. Phys. Chem. Solids 33, 59 (1972).
[17]K. R. Lea, M. J. M. Leask, and W. P. Wolf, J. Phys. Chem. Solids 23, 1381 (1962).

[18]L. Köster, in *Neutron Physics,* Vol. 80 of *Springer Tracts in Modern Physics* (Springer, Berlin, 1977).
[19]E. Holland-Moritz, D. Wohlleben, H. Scheuer, and M. Loewenhaupt, J. Magn. Magn. Mater. 14, 234 (1979).
[20]U. Walter, Diplomthesis University Cologne, 1980 (unpublished), appearing in reports of the Kernforschungsanlage Jülich, Jül-Spez 96 (1981).
[21]C. Stassis and H. W. Deckman, J. Phys. C 9, 2241 (1976).
[22]S. M. Shapiro, J. D. Axe, R. J. Birgeneau, J. M. Lawrence, and R. D. Parks, Phys. Rev. B 16, 2225 (1977).
[23]A. Furrer and H. G. Purwins, J. Phys. C 9, 1491 (1976).
[24]H. W. Ludwigs, U. Häfner, E. Holland-Moritz, W. Zell, B. Roden, and D. Wohlleben, J. Magn. Magn. Mater. 15-18, 607 (1980).
[25]H. W. Ludwigs, Dissertation, University of Cologne, 1981 (unpublished); and W. Zell, Dissertation, University of Cologne, 1981 (unpublished).
[26]B. H. Grier, S. M. Shapiro, C. F. Majkrzak, and R. D. Parks, Phys. Rev. Lett. 45, 666 (1980).
[27]D. Plümacher, Dissertation, University of Cologne, 1980 (unpublished).
[28]G. Krill, L. Abaldi, M. F. Ravet, J. P. Kappler, and A. Meyer J. Phys. (Paris) 41, 1121 (1980).
[29]I. R. Harris and G. V. Raynor, J. Less Common Metals 9, 7 (1965).
[30]K. R. Bauchspiess, W. Boksch, E. Holland-Moritz, H. Launois, R. Pott, and D. Wohlleben, in *Valence Fluctuations in Solids,* edited by L. M. Falicov, W. Hanke, and M. B. Maple (North-Holland, New York, 1981).
[31]J. P. Kappler and A. Meyer, J. Phys. F 9, 143 (1979).
[32]W. C. M. Mattens, F. R. de Boer, A. P. Murani, and G. H. Lander, J. Magn. Magn. Mater. 15-18, 973 (1980).
[33]S. Horn, E. Holland-Moritz, M. Loewenhaupt, F. Steglich, H. Scheuer, A. Benoit, and J. Flouquet, Phys. Rev. B 23, 3171 (1981).
[34]B. Sales and D. Wohlleben, Phys. Rev. Lett. 35, 1240 (1975).
[35]M. Loewenhaupt and E. Holland-Mortiz, J. Magn. Magn. Mater. 9, 50 (1978).
[36]E. Holland-Mortiz and M. Loewenhaupt, J. Phys. (Paris) 40, C5-359 (1979).
[37]C. Stassis, C. K. Loong, B. N. Harmon, S. H. Lui, and R. M. Moon, J. Appl. Phys. 50, 7567 (1979).
[38]A. Bringer and H. Lustfeld, Z. Phys. B 28, 213 (1977); H. Lustfeld and A. Bringer, Solid State Commun. 28, 119 (1978).
[39]D. M. Newns and A. C. Hewson, J. Phys. F 10, 2429 (1980).
[40]G. Neumann, Diplomthesis, University of Cologne, 1981 (unpublished).
[41]R. Schefzyk, Diplomthesis, University of Cologne, 1980 (unpublished).
[42]R. Pott, Dissertation, University Cologne, 1982 (unpublished).
[43]K. R. Bauchspiess, Diplomthesis, University Cologne, 1982 (unpublished).